1480 nm Diode-Pumped Er^{3+}:Yb^{3+} Co-Doped Phospho-Alumino-Silicate Fiber for Extending the L-band Gain up to 1625 nm

Ziwei Zhai and Jayanta K. Sahu

***Abstract*—In this paper, we report erbium/ytterbium (Er/Yb) co-doped phospho-alumino-silicate fibers (EYDFs) fabricated by the modified chemical vapor deposition (MCVD) and solution doping technique, to extend the L-band gain up to 1625 nm. Fibers with different doping concentrations and Yb-to-Er ratios were studied in terms of the spectroscopic properties and optical amplification in the L-band when pumped at 1480 nm. A higher Yb-to-Er ratio suppressed the signal-induced excited-state absorption (ESA) effect and also improved the amplifier gain in the L-band. A maximum gain of 15.5 dB at 1625 nm was achieved for the fiber with an Yb-to-Er ratio of 3.5. The gain coefficient was 0.039 dB/mW and the saturation output power was 21.5 dBm at 1600 nm. On the other hand, one highly doped fiber with the Er_2O_3 concentration of 0.5 mol% and an Yb-to-Er ratio of 2 was demonstrated to have the controlled Er concentration quenching and a reduced amplifier device length, exhibiting 12.9 dB gain and 6.3 dB noise figure (NF) at 1625 nm, with <5.8 dB NF from 1575 to 1623 nm. What's more, the temperature-dependent amplifier performance was studied, over the temperature range of -60 to 80 °C. The temperature-dependent-gain (TDG) coefficient and its zero-point wavelength were reported. An increased L-band gain was achieved by cooling the fiber.**

***Index Terms*—Optical fibers; Erbium-ytterbium co-doped fibers; L-band fiber amplifiers.**

I. Introduction

To support the continuously increasing demand in the telecommunication data transmission capacity, there is a great interest in extending the gain bandwidth of L-band erbium-doped fiber amplifiers (EDFAs) to achieve a wider transmission bandwidth in the lowest-loss wavelength region of the silica fibers. The amplification of EDFAs is based on the stimulated emission from $^4I_{13/2}$ manifolds, from where the excited ions can also be excited to $^4I_{9/2}$ manifolds when absorbing signal photons carrying the energy overlapping with the transition from $^4I_{13/2}$ to $^4I_{9/2}$. This phenomenon is the signal-induced excited state absorption (ESA), resulting in the undesired loss due to non-radiative depletion. Although the peak wavelength of this ESA transition appeared at ~1680 nm, there is a high probability for the ESA tail to extend to shorter wavelengths until ~1590 nm [1]. The ultimate bandwidth limitation of the L-band EDFAs is determined by the signal-induced ESA effect [2], which strongly depends on the glass composition. The intrinsic spectroscopic properties of Er-ions, including the emission, absorption, and ESA cross-sections, can be modified by tailoring the glass composition. Tellurite and antimony-silicate (MCS) glass hosts were studied to red-shift the ESA to extend the L-band gain [2], [3]. Bismuth (Bi) and Er co-doped fibers were studied for the C + L + U band, which still required more investigations on the fiber development to balance the Bi active centers (BACs) in the germanosilicate glass host with a higher concentration of GeO_2 (>50%) [4]. With strong mechanical- and environmental- stability and low loss, phosphorus (P) and/or aluminum (Al) co-doped silicate are the most common glass hosts for EDFs in the current communication systems. It was reported that P/Al co-doped silicate EDFs extended the L-band gain compared to alumino-silicate EDFs [5], [6]. Ytterbium/phosphorus (Yb/P) co-doped silicate EDFs were employed to improve the L-band amplification. Using cladding-pumping and a double-pass amplifier configuration, a gain of 20 dB was achieved at 1620 nm [7]. One core-pumped Er/Yb/P co-doped silicate fiber was reported to extend the L-band amplification to 1623 nm [8]. Recently, it was reported that cerium/phosphorus (Ce/P) co-doped silicate EDFs had no ESA effect until 1620 nm, but only showing the normalized gain range up to 1623 nm [9].

Another limitation in L-band EDFAs is a higher noise figure (NF) compared to C-band EDFAs. For efficient gain in the L-band, a lower Er^{3+} ion population inversion level of ~0.4 is normally used compared to C-band EDFAs with an inversion level of ~0.65 [10]. To achieve sufficient gain, a much longer device length of fiber is required for L-band EDFAs, thus inducing more background loss and amplified spontaneous emission (ASE) effect. One solution is to develop high Er concentration fibers, with the trade-off of a high chance of the Er^{3+} ion clustering and concentration quenching thus degrading the power conversion efficiency (PCE) [11]. Several effective co-dopants were verified to help Er^{3+} uniformly disperse in the

Manuscript received xx xx, xxxx; revised xx xx, xxxx; accepted xx xx, xxxx. Date of publication xx xx, xxxx; date of current version xx xx, xxxx.

The authors are with the Optoelectronics Research Centre, University of Southampton, SO17 1BJ Southampton, U.K. (e-mail: z.zhai@soton.ac.uk; jks@orc.soton.ac.uk). *(Corresponding author: Ziwei Zhai.)*

Color versions of one or more of the figures in this article are available online at https://ieeexplore.ieee.org.

Digital Object Identifier XXXXXXXXXX.

glass matrix with a higher solubility and less clustering effect. Al and P form the solvation shell around Er^{3+} to form well-coordinated state ions with suppressed clustering [12]. With higher efficiency in increasing Er solubility, Al also helps suppress the evaporation of P_2O_5 during the preform fabrication process to inhibit the depressed index in the middle of the refractive index profile [13]. Also, the formation of the $AlPO_4$ unit, similar to the SiO_2 structure, decreases the refractive index difference (*dn*) and increases the PCE in EDFs [14]. By increasing the P-to-Al ratio, Er^{3+} ions are preferentially moved to P-rich sites [15], resulting in the red-shifted emission and ESA spectra to benefit the L-band gain profile. With a very close atomic radius and charge, co-doping with Yb^{3+} effectively suppresses Er concentration quenching by forming clusters between different rare earth (RE) ions without overlapping energy levels [16].

The thermal stability of EDFAs is also an important factor to consider for practical applications as most commercial EDFAs have an operating temperature range from -30 to 65 ºC. Also, considering the extreme environmental temperatures in communication applications, the temperature range from -60 to 80 ºC was used in this work to study the temperature-dependent characteristics of EDFs.

To the best of our knowledge, there are very few reports concerning the highly Er/Yb co-doped P/Al-silicate fiber (EYDF) in extending the L-band gain bandwidth [17]. And there is no report on the temperature-related properties of L-band P/Al-silicate EYDFs. In this paper, we report a set of P/Al-silicate EYDFs in extending the L-band gain up to 1625 nm using bi-directional pumping at 1480 nm. We compared the spectroscopic properties and the gain and NF from 1570 to 1625 nm of EYDFs with different doping concentrations and Yb-to-Er ratios. Emission coefficient, signal-induced ESA, unsaturable loss (UL), gain coefficient, and saturation output power were studied. Also, the temperature-dependent L-band amplifier performance was studied and discussed from -60 to 80 ºC.

TABLE I
BASIC CHARACTERISTICS OF EYDFS IN THIS WORK

	EYDF1	EYDF2	EYDF3
Er_2O_3 (mol%)	0.5	0.2	0.16
Yb_2O_3 (mol%)	1.0	0.7	0.23
Al_2O_3 (mol%)	1.2	0.8	0.5
P_2O_5 (mol%)	12.0	11.0	6.6
Core/cladding (μm)	4.6/125	3.9/125	7/100
Numerical aperture	0.22	0.20	0.14
LP_{11} mode cutoff (nm)	1091	1070	1340
Abs @1535 nm(dB/m)	77	38	22
Abs @1480 nm (dB/m)	22	11	6
UL @1480 nm (%)	11	8.7	8.5
Background loss (dB/m)	0.11	0.13	0.03
Metastable lifetime (ms)	8.8	9.1	9.3

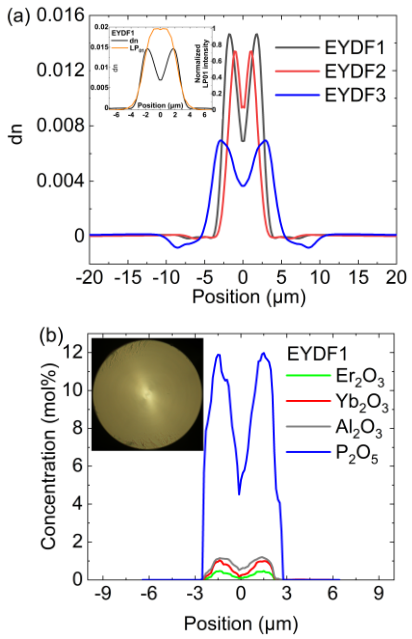

Fig. 1. (a) Refractive index difference (*dn*) for EYDF1, EYDF2, and EYDF3 (the inset shows *dn* and LP_{01} mode field intensity at 1600 nm profiles for EYDF1) and (b) concentration distributions of the core elements (Er_2O_3, Yb_2O_3, Al_2O_3, and P_2O_5) for EYDF1 (the inset shows the cross-sectional view under the microscope).

II. FIBER CHARACTERISTICS

Several Er/Yb co-doped phospho-alumino-silicate preforms were fabricated in-house using the modified chemical vapor deposition (MCVD) technique. Er, Yb and Al were incorporated in the P_2O_5-SiO_2 soot using the solution doping technique [18]. By engineering the level of Er, Yb, Al, and P, three P-dominant glass host EYDFs were selected for comparison with different Er and Yb concentrations. First, several high-purity silica cladding layers were deposited inside a synthetic silica substrate tube (F300 from Heraeus). Next, an unsintered soot layer containing SiO_2 and P_2O_5 was thermophoretically deposited at the temperature of 1450±10 ºC by moving the burner upstream followed by a pre-sintering pass at a temperature of ~1025 ºC. Then, the substrate tube with a porous soot layer was removed from the MCVD lathe and immersed in a methanolic solution containing chlorides of erbium, ytterbium, and aluminum. After a sufficient solution doping period (~1 hour), the dopants saturate the soot and the glassware was reassembled to the lathe. After drying of the soot body, MCVD continued with oxidation, sintering, collapsing and sealing processes, to obtain a solid preform rod. Also, the $POCl_3$ over-doping was used in these processes to suppress the evaporation of phosphorous at high temperatures. During the soot deposition, the flow of precursors was kept the same for EYDF1 and EYDF2, with a $SiCl_4$-to-$POCl_3$ ratio of 1:4, whereas for EYDF3, the $SiCl_4$-to-$POCl_3$ ratio was 1:2. After ~100 mm length of the preform from the beginning of the deposition, the core/cladding refractive index difference (*dn*) was uniformly distributed to, 0.016±0.001 for the preform of EYDF1, 0.015±0.001 for the preform of EYDF2, and ~0.007 for the preform of EYDF3, measured by the preform analyzer

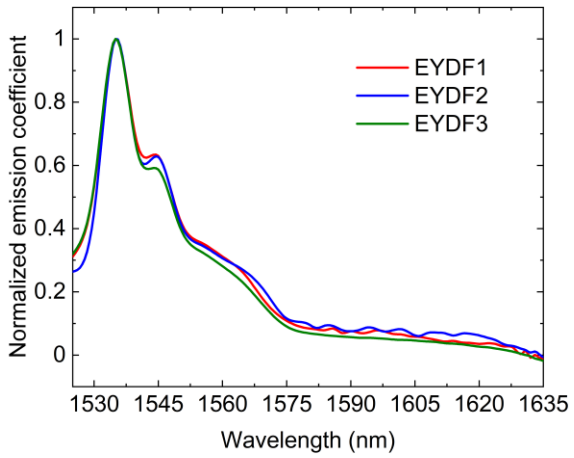

Fig. 2. Normalized emission coefficient spectra of EYDF1, EYDF2 and EYDF3.

(Photon Kinetics, 2600HP). The same section of each preform (150±25 mm from the beginning of the deposition) was selected for further processing for drawing into single-mode fibers with a core/cladding diameter of ~4.6/125 μm for EYDF1, ~3.9/125 μm for EYDF2, and ~7/100 μm for EYDF3. The numerical aperture (NA) was 0.22 for EYDF1, 0.20 for EYDF2, and 0.14 for EYDF3. The measured LP_{11} mode cutoff wavelength was 1091 nm for EYDF1, 1070 nm for EYDF2, and 1340 nm for EYDF3. The measured background loss was 0.11 dB/m for EYDF1, 0.13 dB/m for EYDF2, and 0.03 dB/m for EYDF3. The basic characteristics of the three EYDFs are listed in Table I. The core compositions were obtained from an electron probe micro-analyzer (EPMA). With a P-to-Al ratio of >10, the glass network structure was strongly dominated by P, providing a P-rich local environment for the Er^{3+} and Yb^{3+} ions [15]. Er_2O_3 concentration was 0.5, 0.2 and 0.16 mol% for EYDF1, EYDF2 and EYDF3, respectively. EYDF2 had the highest Yb-to-Er ratio of 3.5, compared to the ratio of 2 for EYDF1 and 1.4 for EYDF3. The refractive index difference (*dn*) profile, the fundamental mode (LP_{01}) field intensity profile at 1600 nm, and the concentration distributions of the core elements (Er_2O_3, Yb_2O_3, Al_2O_3, and P_2O_5) for EYDF1 were illustrated in Fig. 1. The absorption coefficient spectra were measured using the white light source and an optical spectrum analyzer (OSA, YOKOGAWA-AQ6370) by the cut-back method. The Er absorption peak appeared at ~1535 nm with an absorption coefficient of 77 dB/m for EYDF1, 38 dB/m for EYDF2, and 22 dB/m for EYDF3. Then, the variation of the absorption coefficient in EYDFs with increasing launched power from a 1480 nm laser diode (LD) was measured by the cut-back method. The absorption coefficient decreased until the fiber was saturated by the high launched power, reflecting the Er^{3+} ion quenching effect. Unsaturable loss (UL) was calculated using the unsaturable absorption coefficient to small-signal absorption coefficient ratio [19], which was 11% for EYDF1, 8.7% for EYDF2, and 8.5% for EYDF3. There has been no significant increase in UL for EYDF1, although it has a much higher Er concentration, which is more than double and triple the Er concentration of EYDF2 and EYDF3, respectively. It, therefore, indicates that Er^{3+} clustering was well-controlled for highly Er-doped EYDF1. What's more, we calculated the overlap factors of the pump mode (1480 nm) and signal mode (1600 nm) with the erbium doping in the core, based on the measured fiber refractive index profiles. The overlap factor at 1480 nm was calculated to be 0.50 for EYDF1, 0.41 for EYDF2, and 0.58 for EYDF3. The overlap factor at 1600 nm was calculated to be 0.46 for EYDF1, 0.36 for EYDF2, and 0.55 for EYDF3.

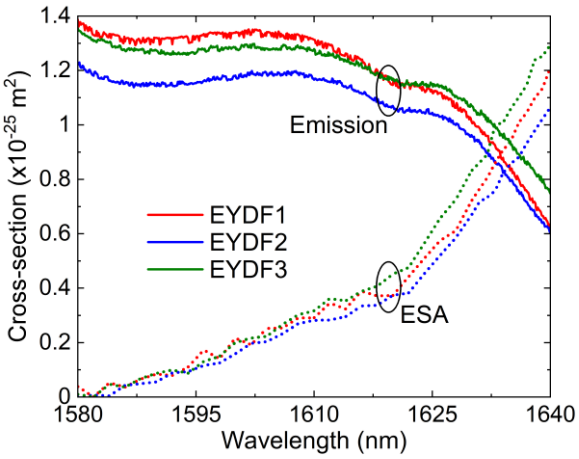

Fig. 3. Emission and excited-state absorption (ESA) cross-sections spectra of EYDF1, EYDF2 and EYDF3.

To evaluate the amplification performance and the ESA effect, we measured the on-off gain from the output signals after the EYDF under the conditions of the pump diode being on and off, respectively. Then, the emission coefficient was obtained according to McCumber theory from the measured absorption coefficient and on-off gain spectra, described by equation (1)-(2) [20].

$$G_{on-off} = 4.343 n_2 \alpha(\lambda) \left\{ 1 + exp\left[\frac{hc}{k_B T} \left(\frac{1}{\lambda_0} - \frac{1}{\lambda} \right) \right] \right\} \quad (1)$$

$$G_{on-off} = 4.343 n_2 \left(\alpha(\lambda) + g^*(\lambda) \right) \quad (2)$$

In which, $G_{on\text{-}off}$ is the on-off gain in dB/m, $\alpha(\lambda)$ is the absorption coefficient, h is the Planck constant, c is the speed of light in vacuum, k_B is the Boltzmann constant, T is the temperature in Kelvin, λ_0 is the wavelength where the absorption and emission coefficients are equal. To obtain the fractional population on the $^4I_{13/2}$ level (n_2), (1) was used in the wavelength range below 1580 nm, where the ESA effect is negligible. Then, (2) was used to obtain the emission coefficient (g^*). Fig. 2 shows the normalized emission coefficient spectra of the three EYDFs. With the highest Yb-to-Er ratio of 3.5, EYDF2 had the highest emission coefficient in the L-band, indicating the potential for extending the L-band gain bandwidth. Also, the slope of the emission coefficient curve in the range from 1570 to 1625 nm was 0.17% for EYDF1, and 0.14% for EYDF2 and EYDF3. The flat emission coefficient was another promising indication of the extended L-band amplification [9]. Then, the emission and absorption cross-

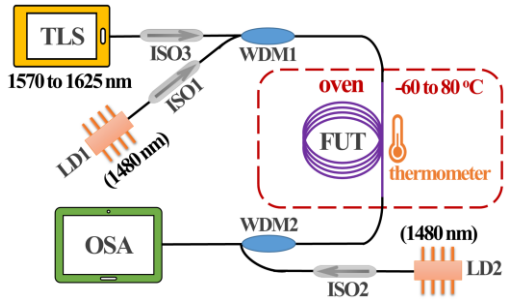

Fig. 4. Schematic of the experimental setup for the L-band EYDFA.

sections (σ_e and σ_a) were calculated based on the Füchtbauer-Ladenburg (FL) equation and McCumber theory [21]. FL equation was used to derive σ_e from the fluorescence intensity spectrum, together with McCumber theory to relate σ_e to σ_a. The on-off gain was used to calculate the ESA cross-section (σ_{ESA}), as equation (3) shows [22]. N_2 is the effective Er concentration on the $^4I_{13/2}$ level. Fig. 3 shows σ_e and σ_{ESA} spectra, with the cross-point appearing at 1633.6 nm for EYDF1, 1634.2 nm for EYDF2, and 1632.6 m for EYDF3. A higher Yb-to-Er ratio red-shifted the cross-point of σ_e and σ_{ESA} and decreased σ_{ESA}, beneficial in extending the L-band gain bandwidth.

$$\sigma_{ESA} = \sigma_e + \sigma_a - \frac{G_{on-off}}{4.343 N_2} \quad (3)$$

III. L-BAND AMPLIFICATION CHARACTERISTICS

The schematic of the experimental setup for the L-band EYDFA is illustrated in Fig. 4. A tunable laser source (TLS, 8164A Lightwave measurement system, Agilent) was used to provide the signal power of -25 dBm covering the wavelength range of 1570-1625 nm. Two LDs operating at 1480 nm (3SP Technologies) were used for bi-directional in-band pumping, without the overlap with any absorption bands of Yb^{3+} ions. The maximum output power was 750 mW from the co-propagating pump LD1 and 450 mW from the counter-propagating pump LD2. Three isolators (ISOs, OFR) were used to protect the TLS and LDs from the backward propagation of signal and pump light, respectively. Two wavelength division multiplexers (WDMs, Lightel) were used to combine and couple the signal and pumps. An OSA (YOKOGAWA-AQ6370) was used to capture the input and amplified signal spectra. SMF-28 was used for launching the signal and pump into the FUT and collecting the output signal after the amplifier. To characterize the temperature-dependent performance, the fiber under test (FUT) was placed in an oven with a thermometer to monitor the temperature. Fig. 5 shows the gain and NF for EYDF1, EYDF2, and EYDF3 at room temperature (RT, ~22 °C), using the optimized fiber length with respect to the maximum gain from 1610 nm to 1625 nm, which was 23 m for EYDF1, 62 m for EYDF2, and 62 m for EYDF3. The average splice loss at the signal wavelengths between the FUT and the conventional SMF-28 was within the range of 0.16±0.06 dB for EYDF1, 0.04±0.01 dB for EYDF2, and 0.04±0.01 dB for EYDF3. The splice loss at the 1480 nm pump wavelength was within the range of 0.29±0.05 dB for EYDF1, 0.09±0.02 dB for EYDF2 and 0.10±0.04 dB for EYDF3. The difference in the splice losses for the three EYDFs was from the difference in the core

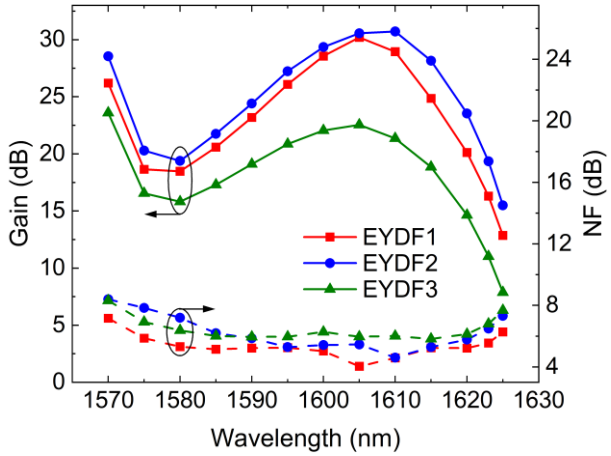

Fig. 5. Gain and NF spectra at RT of EYDF1 (23 m), EYDF2 (62 m) and EYDF3 (62 m) for an input signal power of -25 dBm using the 1480 nm co-propagating pump power of 750 mW and counter-propagating pump power of 450 mW.

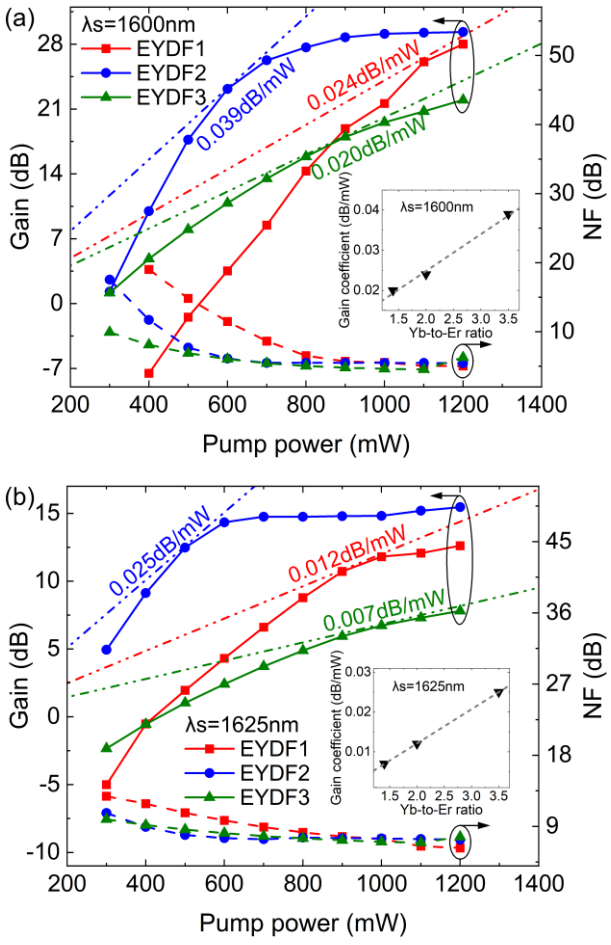

Fig. 6. Gain and NF at (a) 1600 nm and (b) 1625 nm variations with the total launched pump power of EYDF1 (23 m), EYDF2 (62 m) and EYDF3 (62 m) at RT (the inset shows the gain coefficient variations with the Yb-to-Er ratio at 1600 and 1625 nm, respectively).

diameter and NA. It was observed that the gain increased with the Yb-to-Er ratio in the fiber. EYDF1 and EYDF2 achieved ~30 dB gain at 1605 nm and EYDF2 achieved a higher overall gain than EYDF1. At 1625 nm, EYDF2 exhibited 15.5 dB gain and 7.3 dB NF, while EYDF1 exhibited 12.9 dB gain and 6.3 dB NF. In the 53 nm bandwidth from 1570 to 1623 nm, EYDF2 exhibited >19 dB gain with 6.4±1.8 dB NF. The highest gain achieved at longer wavelengths for EYDF2 was mainly due to its higher Yb-to-Er ratio of 3.5 and the red-shifted cross-point of σ_e and σ_{ESA} of 1634.2 nm. With the lowest Yb-to-Er ratio of 1.4 and cross-point of σ_e and σ_{ESA} of 1632.6 nm, EYDF3 only exhibited 7.8 dB gain and 7.6 dB NF at 1625 nm. With a higher Er concentration, EYDF1 benefited from its reduced device length thus obtaining the lowest NF, achieving <7 dB NF in the range of 1570-1625 nm and <5.8 dB NF in the range of 1575-1623 nm. In the case of uniform inversion, the population inversion level ($N_2/(N_1+N_2)$) was calculated as 44% for EYDF1, 37% for EYDF2, and 42% for EYDF3, derived from equation (4)-(5) [23].

$$n_{sp} = \frac{\sigma_e N_2}{\sigma_e N_2 - \sigma_a N_1} \tag{4}$$

$$n_{sp} = \frac{F_0 G - 1}{2(G-1)} \tag{5}$$

In which, n_{sp} is the spontaneous emission factor, as a function of the population inversion in the gain medium. N_1 and N_2 are the ion populations of the $^4I_{15/2}$ and $^4I_{13/2}$ levels. F_0 and G are the noise figure and gain in the linear unit.

Then, the gain and NF variations with the total pump power were measured, as shown in Fig. 6. The gain coefficient, defined as the highest gain-to-pump power ratio, was 0.024, 0.039, and 0.020 dB/mW at 1600 nm and 0.012, 0.025, and 0.007 dB/mW at 1625 nm for EYDF1, EYDF2, and EYDF3, respectively. The gain coefficient linearly increased with the Yb-to-Er ratio, as the insets of Fig. 6 show. Next, we measured the gain and NF variations with the TLS input signal power increasing from -35 to 0 dBm. The maximum input signal power was limited to 0 dBm by the TLS used in this work. As Fig. 7(a) shows, at 1600 nm, the gain increased as the signal power decreased. The saturation output power was defined as the output signal power where the gain has dropped by 3 dB compared with the small-signal gain value. The saturation output power was 11.6, 21.5, and 4 dBm for EYDF1, EYDF2, and EYDF3, respectively. As Fig. 7(b) shows, at 1625 nm, the gain exhibited a much less variation with the signal power, which was 12.1 ± 0.8, 15.3 ± 0.2, 7.7 ± 0.1 dB for EYDF1, EYDF2, and EYDF3, respectively.

Furthermore, we measured the temperature dependence of the gain and NF from -60 to 80 ºC for EYDF1 and EYDF2. We haven't presented the temperature-dependent gain and NF for EYDF3 due to its lower gain performance in the L-band. Fig. 8 shows the temperature-dependent-gain (TDG) coefficient, defined as the linear regression fitting coefficient between the gain and temperature. The zero-point wavelength of the TDG coefficient appeared at ~1573 nm for EYDF1 and ~1595 nm for

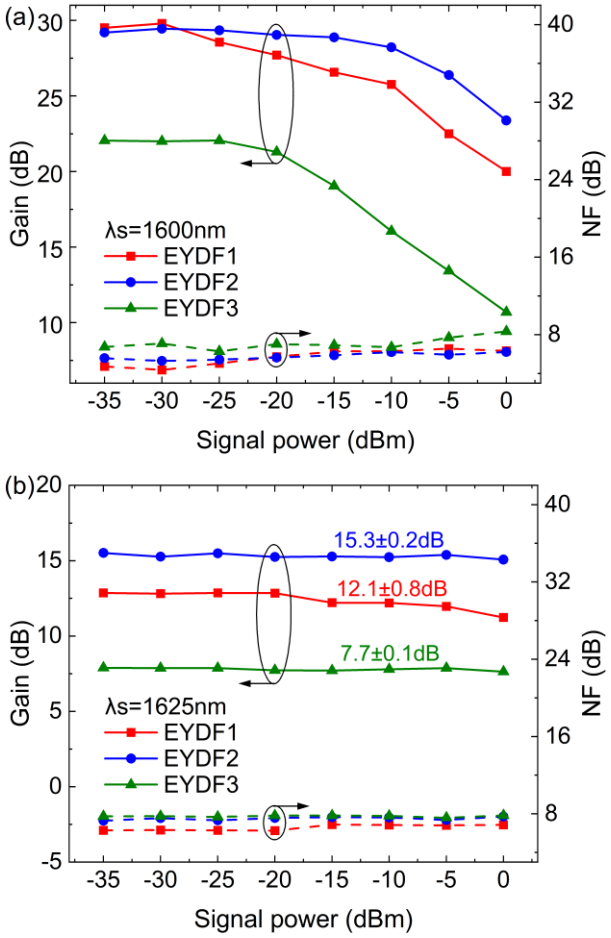

Fig. 7. Gain and NF at (a) 1600 nm and (b) 1625 nm variations with the input signal power of EYDF1 (23 m), EYDF2 (62 m) and EYDF3 (62 m) at RT.

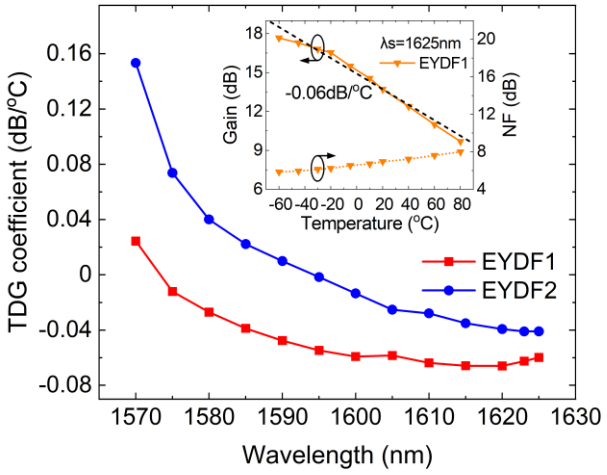

Fig. 8. Temperature-dependent gain (TDG) coefficient spectra of EYDF1 (23 m) and EYDF2 (62 m) (inset shows the gain and NF variations with the temperature at 1625 nm of EYDF1).

EYDF2. Beyond the zero-TDG coefficient point, gain increased as the temperature decreased. By cooling the fiber, the increase of σ_a at shorter wavelengths increased the pumping efficiency and the decrease of σ_a at longer wavelengths suppressed the L-band signal re-absorption, thus benefiting the gain at longer wavelengths [24]. According to Boltzmann's law, the Er ion

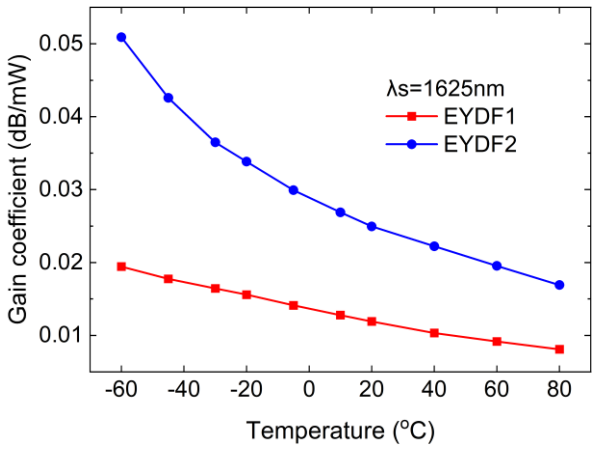

Fig. 9. Gain coefficient at 1625 nm variations with the temperature of EYDF1 (23 m) and EYDF2 (62 m).

populations were thermalized and de-populated to lower energy sub-levels at a lower temperature. The dominant gain waveband red-shifted under a lower inversion level, which was more beneficial to the L-band gain compared to the C-band [10]. Also, the less populated excited state contributed to less ESA loss to benefit the L-band amplification. What's more, the narrowed σ_e and σ_{ESA} spectra at a lower temperature reduced the overlap and achieved a red-shifted cross-point of σ_e and σ_{ESA}, with suppressed ESA effect to help the L-band gain [25]. As a result, by decreasing the temperature to -60 °C, gain at 1625 nm was increased to 18 dB for EYDF1 and 17.1 dB for EYDF2, using the maximum pump power (i.e., co-propagating pump power of 750 mW and counter-propagating pump power of 450 mW). NF at 1625 nm was 5.8 dB for EYDF1 and 6.7 dB for EYDF2. The TDG coefficient at 1625 nm was -0.06 dB/°C for EYDF1 and -0.04 dB/°C for EYDF2. What's more, the gain variation with the pump power was measured to calculate the gain coefficient at different temperatures for EYDF1 and EYDF2, as shown in Fig. 9. The gain coefficient increased as the temperature dropped, achieving 0.02 dB/mW at 1625 nm for EYDF1 at -60 °C. EYDF2 had a gain coefficient of 0.051 dB/mW at 1625 nm at -60 °C.

IV. Conclusion

In conclusion, we fabricated a set of Er/Yb co-doped phospho-alumino-silicate fibers with different doping concentrations and Yb-to-Er ratios. We demonstrated the L-band EYDFA up to 1625 nm pumped by 1480 nm diodes. The spectroscopic characteristics and amplifier gain and NF were measured and analyzed for different EYDFs. By tailoring the glass compositions, one high-concentration EYDF1 with the Er peak absorption coefficient of 77 dB/m was demonstrated with the controlled Er concentration quenching and signal-induced ESA effects, advantageous in the extended L-band operation with a reduced device length. The 23 m piece of EYDF1 obtained 12.9 dB gain and 6.3 dB NF at 1625 nm, with <5.8 dB NF from 1575 to 1623 nm. A high Yb-to-Er ratio of 3.5 for EYDF2 was studied to extend the L-band gain, achieving 15.5 dB gain at 1625 nm and >19 dB gain from 1570 to 1623 nm. Also, a higher Yb-to-Er ratio improved the gain coefficient and saturation output power, suppressed the ESA effect, and red-shifted the cross-point of emission and ESA cross-sections. At 1600 nm, EYDF2 achieved the gain coefficient of 0.039 dB/mW and the saturation output power of 21.5 dBm. At 1625 nm, a negligible gain variation was observed with the input signal power varying from -35 to 0 dBm. Furthermore, the temperature-dependent amplifier characteristics were studied from -60 to 80 °C, showing the increased L-band gain and gain coefficient at a lower temperature.

Acknowledgment

The data for this work can be accessed at the University of Southampton Institutional Research Repository doi: https://doi.org/10.5258/SOTON/D2311.

References

[1] M. Bolshtyansky, I. Mandelbaum, and F. Pan, "Signal excited-state absorption in the L-band EDFA: Simulation and measurements," *IEEE J Lightwave Technol.*, vol. 23, no. 9, pp. 2796-2799, 2005.

[2] A. Mori, T. Sakamoto, K. Kobayashi, *et al.*, "1.58-μm broad-band erbium-doped tellurite fiber amplifier," *IEEE J Lightwave Technol.*, vol. 20, no. 5, pp. 822-827, 2002.

[3] A. J. G. Ellison, D. E. Goforth, B. N. Samson, *et al.*, "Extending the L-band to 1620 nm using MCS fiber," in *OFC*, San Diego, California, United States, paper TuA2.1, 2001.

[4] S. V. Firstov, K. E. Riumkin, A. M. Khegai, *et al.*, "Wideband bismuth- and erbium-codoped optical fiber amplifier for C+ L+ U-telecommunication band," *Laser Phys. Lett.*, vol. 14, no. 11, p. 110001, 2017.

[5] S. Tanaka, K. Imai, T. Yazaki, *et al.*, "Ultra-wideband L-band EDFA using phosphorus co-doped silica-fiber," in *OFC*, San Diego, California, United States, paper ThJ3, 2002.

[6] Z. Zhai, A. Halder, M. Núñez-Velázquez, *et al.*, "Temperature-Dependent Study on L-Band EDFA Characteristics Pumped at 980 nm and 1480 nm in Phosphorus and Aluminum-Rich Erbium-Doped Silica Fibers," *IEEE J Lightwave Technol.*, vol. 40, no. 14, pp. 4819-4824, 2022.

[7] C. Codemard, D. B. S. Soh, K. Ylä-Jarkko, *et al.*, "Cladding-pumped L-band phosphosilicate erbium-ytterbium co-doped fiber amplifier," in *OAA*, paper TuC2, 2003.

[8] Y. Chen, Y. Lou, Z. Gu, *et al.*, "Extending the L-band amplification to 1623 nm using Er/Yb/P co-doped phosphosilicate fiber," *Opt. Lett.*, vol. 46, no. 23, pp. 5834-5837, 2021.

[9] Y. Lou, Y. Chen, Z. Gu, *et al.*, "Er^{3+}/Ce^{3+} Co-doped Phosphosilicate Fiber for Extend the L-band Amplification," *IEEE J Lightwave Technol.*, vol. 39, no. 18, pp. 5933-5938, 2021.

[10] J. Minelly, and A. Ellison, "Applications of antimony–silicate glasses for fiber optic amplifiers," *Optical Fiber Technology*, vol. 8, no. 2, pp. 123-138, 2002.

[11] W. J. Miniscalco, "Erbium-doped glasses for fiber amplifiers at 1500 nm," *IEEE J Lightwave Technol.*, vol. 9, no. 2, pp. 234-250, 1991.

[12] K. Arai, H. Namikawa, K. Kumata, *et al.*, "Aluminum or phosphorus co-doping effects on the fluorescence and structural properties of neodymium-doped silica glass," *J. Appl. Phys.*, vol. 59, no. 10, pp. 3430-3436, 1986.

[13] G. G. Vienne, W. S. Brocklesby, R. S. Brown, *et al.*, "Role of Aluminum in Ytterbium-Erbium Codoped Phosphoaluminosilicate Optical Fibers," *Opt. Fiber Technol.*, vol. 2, no. 44, pp. 387-393, 1996.

[14] M. E. Likhachev, M. M. Bubnov, K. V. Zotov, *et al.*, "Effect of the $AlPO_4$ join on the pump-to-signal conversion efficiency in heavily Er-doped fibers," *Opt. Lett.*, vol. 34, no. 21, pp. 3355-3357, 2009.

[15] C. Shao, F. Wang, Y. Jiao, *et al.*, "Relationship between glass structure and spectroscopic properties in Er^{3+}/Yb^{3+}/Al^{3+}/P^{5+}-doped silica glasses," *Opt. Mater. Express*, vol. 10, no. 5, pp. 1169-1181, 2020.

[16] N. V. Kiritchenko, L. V. Kotov, M. A. Melkumov, *et al.*, "Effect of ytterbium co-doping on erbium clustering in silica-doped glass," *Laser Phys.*, vol. 25, no. 2, p. 025102, 2015.

[17] Z. Zhai and J. K. Sahu, "Extending L-Band Gain to 1625 nm Using Er^{3+}:Yb^{3+} Co-Doped Silica Fibre Pumped by 1480 nm Laser Diodes," in *ECOC*, paper Th2A.2, 2022.
[18] J. K. Sahu, Y. Jeong, D. J. Richardson, *et al.*, "A 103 W erbium–ytterbium co-doped large-core fiber laser," *Opt. Commun.*, vol. 227, no. 1-3, pp. 159-163, 2003.
[19] M. P. Kalita, S. Yoo, and J. K. Sahu, "Bismuth doped fiber laser and study of unsaturable loss and pump induced absorption in laser performance," *Opt. Express*, vol. 16, no. 25, pp. 21032-21038, 2008.
[20] H. Feng, S. Jalilpiran, F. Maes, *et al.*, "Characterization of Giles parameters for extended L-band erbium-doped fibers," *J. Opt. Soc. Am. B*, vol. 39, no. 7, pp. 1783-1791, 2022.
[21] W. J. Miniscalco, and R. S. Quimby, "General procedure for the analysis of Er^{3+} cross sections," *Opt. Lett.*, vol. 16, no. 4, pp. 258-260, 1991.
[22] J. E. Román, M. Hempstead, C. Ye, *et al.*, "1.7 μm excited state absorption measurement in erbium-doped glasses," *Appl. Phys. Lett.*, vol. 67, no. 4, pp. 470-472, 1995.
[23] E. Desurvire, "Analysis of noise figure spectral distribution in erbium doped fiber amplifiers pumped near 980 and 1480 nm," *Appl. Opt.*, vol. 29, no. 21, pp. 3118-3125, 1990.
[24] J. L. Gouët, J. Oudin, P. Perault, *et al.*, "On the Effect of Low Temperatures on the Maximum Output Power of a Coherent Erbium-Doped Fiber Amplifier," *IEEE J Lightwave Technol.*, vol. 37, no. 14, pp. 3611-3619, 2019.
[25] T. F. Yao, R. Steinborn, A. S. Webb, *et al.*, "Analysis of noise figure spectral distribution in erbium doped fiber amplifiers pumped near 980 and 1480 nm," in *SumSession*, paper Tu12, 2011.